Bioactive Materials 5 (2020) 938–948

Contents lists available at ScienceDirect

Bioactive Materials

journal homepage: http://www.keaipublishing.com/biomat

Osteoblast/fibroblast coculture derived bioactive ECM with unique matrisome profile facilitates bone regeneration

Mei Li[a,b], Anqi Zhang[a], Jiajing Li[a], Jing Zhou[a], Yanan Zheng[a], Chi Zhang[c], Dongdong Xia[c], Haijiao Mao[d], Jiyuan Zhao[a,*]

[a] Zhejiang Key Laboratory of Pathophysiology, Medical School in Ningbo University, Ningbo, Zhejiang, PR China
[b] Ningbo Institute of Medical Sciences, Ningbo, Zhejiang, PR China
[c] Orthopedic Department, Ningbo First Hospital, Ningbo, Zhejiang, PR China
[d] Department of Orthopaedic Surgery, The Affiliated Hospital of Medical School, Ningbo University, Ningbo, Zhejiang, PR China

ARTICLE INFO

Keywords:
Cell coculture
Bioactive ECM
Matrisome
Bone mimetic microenvironment
Bone regeneration

ABSTRACT

Extracellular matrix (ECM) with mimetic tissue niches was attractive to facilitate tissue regeneration *in situ* via recruitment of endogenous cells and stimulation of self-healing process. However, how to engineer the complicate tissue specific ECM with unique matrisome *in vitro* was a challenge of ECM-based biomaterials in tissue engineering and regenerative medicine. Here, we introduced coculture system to engineer bone mimetic ECM niche guided by cell-cell communication. In the cocultures, fibroblasts promoted osteogenic differentiation of osteoblasts via extracellular vesicles. The generated ECM (MN-ECM) displayed a unique appearance of morphology and biological components. The advantages of MN-ECM were demonstrated with promotion of multiple cellular behaviors (proliferation, adhesion and osteogenic mineralization) *in vitro* and bone regeneration *in vivo*. Moreover, proteomic analysis was used to clarify the molecular mechanism of MN-ECM, which revealed a specific matrisome signature. The present study provides a novel strategy to generate ECM with tissue mimetic niches via cell-cell communication in a coculture system, which forwards the development of tissue-bioactive ECM engineering along with deepening the understanding of ECM niches regulated by cells for bone tissue engineering.

1. Introduction

Tissue lost caused by disease, trauma or congenital abnormalities is often beyond self-healing and required transplantation to replace missing form and function [1,2]. Though auto-transplantation is considered as the “gold standard”, the high risk of donor site morbidity and limited source of donor tissues still restricted its application in clinic [3]. To address this issue, tissue engineering was developed to recreate functional biological replacement tissues and organs for their damaged counterparts via constructions of biomaterials and signaling cues [4,5]. Among these, the tissue microenvironment has emerged as a key determinant of cell behavior and function for the development of functional and biomimetic materials [6]. The engineered constructs should provide physical support and biological signals, as well as mobilized endogenous cells for tissue repair [1,2]. Based on these, naturally derived materials with appropriate microenvironment are attractive due to their biophysical and biochemical cues, and their potential in modulation of cell-cell and cell-extracellular matrix (ECM) interactions [4,7–10].These biomaterials providing physiological fashion have been drawn attention as a new generation of biomaterial and biomaterial modification for tissue engineering to induce the formation of functional tissue by harnessing endogenous regenerative capacity *in situ* [3,11].

ECM, secreted by multiple cells in tissues or organs, is a naturally fibrous network of proteins, glycosaminoglycans and proteoglycans precisely arranged in a tissue-specific 3D architecture and provides specialized local microenvironments [12]. Increasing evidences demonstrated advantages of ECM in tissue engineering and regenerative medicine [3,12,13]. Intrinsic biochemical and mechanical cues in ECM regulated cell phenotype and function in development, in homeostasis and in response to injury [12,14]. Communications between endogenous cells and matrix directed the process of tissue regeneration [15–17]. However, the challenge of ECM-based biomaterials is what kind of ECM is the most suitable for specific tissue regeneration and

Peer review under responsibility of KeAi Communications Co., Ltd.
* Corresponding author. Medical School, Ningbo University, 818 Fenghua Road, Ningbo, Zhejiang, 315211, China.
E-mail address: zhaojiyuan@nbu.edu.cn (J. Zhao).

https://doi.org/10.1016/j.bioactmat.2020.06.017
Received 14 April 2020; Received in revised form 15 June 2020; Accepted 23 June 2020

how to obtain the ECM preserving the tissue specific biochemical composition and ultra-structure to promote the formation of functional tissues for clinical application. Many efforts have been made, including ECM fabrication from different kinds of cell culture, or from whole tissues and organs [18]. Compared with tissue-derived ECM, cell-culture-derived ECM shows faster, easier, cheaper production and more controllable pattern [19]. Less vigorous decellularization also made much more preservation of ECM composition/structure in cell-culture-derived ECM.

Though ECM from various cells (such as human dermal fibroblasts, pre-osteoblasts and BMSCs) have been applied to coat biomaterials for tissue engineering [12,14], the physiological niche *in vivo* should be a complex system which is comprised of complex ECM affected by cell-cell signaling networks, and further guides multi cellular tissue self-organization and regeneration [20,21]. ECM from single type of cells is hard to mimic tissue microenvironment without cell-cell signaling interactions. While it's common to understand that cellular neighborhoods during cell interactions influence cell behavior and have importance to stem cell biology and regeneration [21–24], the influence of cell-cell communication on ECM organization and the role of the generated ECM on tissue regeneration was rarely investigated. Coculture system provides a possible way to investigate cell communication in direct or indirect manners [25–27].

Bone remodeling is a highly coordinated process involving communication between multiple cell types present in the bone tissue, including osteoblasts, osteoclasts, fibroblasts, endothelial cells and immune cells [28]. Amongst them osteoblasts forming a continuous membrane surrounding bone secrete bone organic matrix and control the matrix environment for mineralization [29]. Osteoblasts at the apical membrane continuously communicate with outsides, including multiple cell communication and signaling transportation, which finally influence bone remodeling and bone regeneration *in vivo*. One of these influences should be fibroblasts, which are abundant around osteoblasts in bone tissue and mass accumulated at the beginning of bone regeneration. Moreover, ECM secreted by fibroblasts has also been demonstrated to promote tissue regeneration, including muscle, nerve, artery and bone tissue [3,30]. However, the communication between osteoblasts and fibroblasts and ECM secreted by them were rarely reported.

Here, we cocultured osteoblasts and fibroblasts at different ratios directly to generate complicated ECM to mimic bone local microenvironment. Arrangement and cell-cell communication between two cell types were monitored during coculturing. Structure and matrisome composition of the complicated bone mimetic ECM (BM-ECM) were characterized comprehensively. The effect of BM-ECM on cell proliferation, cell adhesion and osteogenic differentiation were investigated respectively. Moreover, SIS scaffolds coated with BM-ECM were implanted into mouse calvarial defects to assess the ability of BM-ECM for bone regeneration *in vivo*.

2. Materials and methods

2.1. Cell culture and generation of decellularized ECM

MC3T3-E1 cells were cultured in αMEM medium supplemented with 10% fetal bovine serum and penicillin (100U/ml)-streptomycin (0.1 mg/ml). NIH/3T3 cells were cultured in DMEM medium supplemented with 10% bovine calf serum, 0.1 mM NEAA (non essential amino acid) and penicillin (100U/ml)-streptomycin (0.1 mg/ml). To obtain the coculture of MC3T3-E1 and NIH/3T3 cells (MC/NIH cocultures), these two kinds of cells were typsinized into single cells and mixed together in coculture medium (MC3T3-E1 medium:NIH/3T3 medium = 1:1, v/v) at the density of 1.6×10^5 cells/ml with different ratios of cell number (MC3T3-E1:NIH/3T3 = 9:1, 7:3, 5:5, 3:7, 1:9). The mixed cells were seeded and cultured in tissue culture plates for 10 days. Fresh medium was changed every other day.

Decellularized ECM from MC3T3-E1, MC/NIH cocultures and NIH/3T3 cells was prepared following the decellularization process as reported previously [19]. Briefly, Cells were treated with pre-heated triton X-100 at 37 °C for 5 min, and washed with PBS for 3 times. After that, cells were frozen at −80 °C for 40 min and thawed in pre-heated PBS at 37 °C for 40 min, following with PBS washing for 3 times. The freeze/thaw (−80 °C/37 °C) cycles was repeated twice again. All samples were treated with DNase (50 U/ml)/RNase (50 μg/ml) for 2 h at 37 °C, and subsequently washed with PBS for 3 times.

2.2. Gene expression assay (mRNA and protein)

Total mRNA isolation and real-time qPCR performance were operated as previously reported [31]. Briefly, cells were rinsed with PBS and lysed in RNA-Solv Reagent (R6830-02, Omega, Guangzhou, China) according to the manufacturer's instruction. The concentration and purity of mRNA were assessed by UV absorbance at 230 nm, 260 nm and 280 nm using a microplate spectrophotometer. The first-strand cDNA was synthesized using the TransScript One-Step gDNA Removal and cDNA Synthesis SuperMix kit (TransGen Biotech Co. Ltd, Beijing, China). The relative gene expression on mRNA level was assessed by real-time qPCR with SYBR reagent from TransGen Biotech Co. Ltd and calculated by comparative Ct method ($2^{-(\Delta\Delta C(t))}$). Actin was introduced as an internal control.

Alkaline phosphatase (ALP) staining was used to assay the activity level of ALP protein in cells as described previously [31]. Immunofluorescence staining (IF) was used to visualize protein distribution pattern and protein expression level. Primary antibodies for COL1A1 (ab21286, Abcam, Shanghai, China) and Ocn (ab93876, Abcam) were used. F-actin for cell adhesion assay was stained by phalloidin (Beijing Solarbio Science & Technology Co., Ltd, China) following the manufacturer's instruction. Working solution of phalloidin was 150 nM. Secondary antibodies conjugated with Alexa Fluor® 555 or Alexa Fluor® 488 (CST, Shanghai, China) were applied. DAPI was used to show nuclei, and antifade solution was used for sample stocking.

2.3. Fluorescence protein labeling and cell-cell communication assay

To identify the intercellular communication between fibroblasts and osteoblasts, green fluorescence protein (GFP) and red fluorescence protein (RFP) were used to label cells. MC3T3-E1 and NIH/3T3 cells were cultured on a 24-well plate at the density of 3×10^4 cells/well. On next day, 300 μL fresh medium were added into each well, following with 1 μL auxiliary transfection reagent and 10 μL lentivirus containing GFP or RFP expression sequence (ViGene Biosciences, Shangdong, China). Three days later, the labeling cells were passaged and selected by puromycin (MC3T3-E1, 8 μg/ml; NIH/3T3, 2 μg/ml) for 7 days. GFP-MC3T3-E1 and RFP-NIH/3T3 were imaged under fluorescence microscope.

To investigate intercellular communication in MC/NIH cocultures, flow cytometry and transwell-cell culture were introduced. For flow cytometry, GFP-MC3T3-E1 and RFP-NIH/3T3 were cocultured at the ratio of 9:1 (MC:NIH, cell number). The cells in four groups (GFP-MC3T3-E1, RFP-NIH/3T3 and labeled MC/NIH cocultures on day 1 or day 10) were seeded into 6-well plate. The cell density was 1.6×10^5 cells/ml and 2 ml cell suspension solution was added into each well. The cells were typsinized into single cells after culturing and run in a flow cytometer (CytoFLEX, BECKMAN COULTER, CA, USA). The results were analyzed with Flowjo software. For transwell-cell culture, GFP-MC3T3-E1 cells were cultured on the wells in a 24-well plate, while RFP-NIH/3T3 cells were cultured in transwells. Reversely, RFP-NIH/3T3 cells on a 24-well plate and GFP-MC3T3-E1 cells in transwells were performed. The cells on plates were imaged under fluorescence microscope on desired time.

2.4. Morphology of ECM assay

Scanning electron microscope (SEM) and atomic force microscope (AFM) were used to observe the surface of ECM. Samples were fixed in 4% paraformaldehyde PBS for 30 min at room temperature, following with PBS washing. After that, the samples were dehydrated in 50%, 70%, 90%, 95% and 100% ethanol for 15 min each, and dried in a frozen vacuum. For SEM scanning, the samples were sputter-coated with platinum and examined under an SEM (SU-70, Hitachi, Japan). AFM (Oxford Instruments, Cypher S) was utilized to determine the height of ECM surface.

2.5. Quantification of ECM proteins and glycosaminoglycans (GAG)

The total ECM proteins, collagen proteins and GAG were quantified respectively. The ECM from decellularized cells was mechanically detached from tissue culture plates, and UA buffer (8 M urea, 150 mM Tris-HCl, pH8.0) was added to lyse the ECM pallet under agitation at 37 °C for 2 h. After cooling, the lysate was sonicated (80W, 10 s on/15 s off, 10 cycles), and then boiled for 15 min. After centrifuged at 14,000 g for 40 min, the supernatant were transferred to a new tube and quantified with BCA Protein Assay Kit (Bio-Rad, USA).

Collagenous proteins were stained and quantified by Sirius Red/Fast Green collagen staining kit (Chondrex, Inc.) as previously [19]. ECM in a 24-well plate was fixed in Kahle fixative (26.7% ethanol/3.7% formaldehyde/2% glacial acetic acid in distilled water) for 10 min at RT, stained with dye solution for 30 min at RT, and eluted with dye extraction buffer in the kit. OD540 and OD605 was measured and used to calculate the amount of collagen proteins.

For GAG content quantification, cells were cultured on a 24-well plate and decellularized. GENMED GAG quantification kit via DMMB (GENMED scientifics Inc., Wilmington, DE) was used to determine GAG content in ECM according to the manufacturer's instructions. Standard GAG samples in the kit were assayed in the meantime to prepare a standard curve.

2.6. Preparation of ECM/SIS scaffolds

Small intestinal submucossa (SIS), a natural collagenous ECM, was used as an ideal biomaterial with multiple modifications for bone tissue engineering in our previous papers [32–36]. In the present study, we also introduced SIS scaffold as a basic biomaterial to investigate the effects of coculture-ECM on bone regeneration *in vivo*. First, SIS scaffolds were cut into round constructs measuring 4 mm in diameter by biopsy punches. Lyophilized SIS scaffolds (Cook Biotech, Inc., Weat Lafayette, IN) were rehydrated in complete culture medium for at least 24 h before cell culture. MC3T3-E1, MC/NIH and NIH/3T3 cells were seeded on SIS scaffolds in 96-well plates at 5×10^4 cells/well and cultured for 10 days. M-ECM/SIS, MN-ECM/SIS and N-ECM/SIS scaffolds were obtained after decellularization and stored at −80 °C.

2.7. Mouse calvarial defect model

Healthy adult male C57 mice (8 week) were purchased from SFP Biotechnology Co., Ltd. (Beijing, China). The mice were randomly divided into three groups (n = 5). The animals were anesthetized by an intraperitoneal injection of sodium pentobarbital (1%, 50 mg/kg) on a super clean bench. Critical-sized (4 mm) defects were created on the skull, following with implantation of different scaffolds. The mice were sacrificed at 3 and 6 weeks. After that, the skulls were collected surgically and fixed in formaldehyde (4%) overnight. Soft X-ray photographs were taken for radiological analysis under IVIS® Lumina XRMS Series III.

2.8. Ethical statement

All experimental procedures involving animals in this study were conducted in compliance with the Chinese legislation regarding the use and care of laboratory animals and were approved by the Animal Care and Use Committee of Ningbo University.

2.9. Sample harvesting and histological staining

The samples were rinsed with PBS and decalcified in 10% (w/v) sodium citrate/22.5% (v/v) formic acid (Morse's solution) for 2 days, neutralized with 5% sodium sulfate for 6 h, and washed with water for 6 h. The samples were then dehydrated, embedded in paraffin, and sectioned (5 μm). Hematoxylin and eosin (H&E) staining was performed under standard procedures. Masson's trichrome staining (MTS) was performed according to the manufacturer's instructions of staining kit (Solarbio).

2.10. Tandem mass tag (TMT) technology for quantitative proteomic analysis

TMT labeled technology could provide a better understanding of the relative expression levels of proteins and proportion of different components in different groups as a whole. ECM from MC3T3-E1, MC/NIH cocultures and NIH/3T3 were carefully scrapped from 6 cm plates, and lysed in UA buffer as described in the method of total ECM proteins quantification. The dissolved ECM solution was filtered with 0.22 μm filters and stored at −80 °C. The proteins were separated on a SDS-PAGE gel and visualized by coomassie blue staining. After that, the proteins were undergoing enzymolysis process following filter-aided sample preparation (FASP digestion) [37]. Peptide mixture of each sample (100 μg) was labeled using TMT reagent according to the manufacturer's instructions (Thermo Fisher Scientific). Pierce high pH reversed-phase fractionation kit (Thermo) was used to fractionate TMT-labeled digest samples into 10 fractions by an increasing acetonitrile step-gradient elution. Each fraction was injected for nano LC-MS/MS analysis on a Q Exactive mass spectrometer (Thermo) which was coupled to Easy nLC (Thermo) for 90 min. MS/MS spectra were investigated with MASCOT engine (Matrix Science, London, UK) embedded into Proteome Discoverer 1.4. For GO mapping and functional annotation, the protein sequences of differentially expressed proteins were retrieved from UniProtKB database and locally explored against SwissProt database (mouse). Normalization (−1, 1) of the studied protein relative expression data was used to performing hierarchical clustering analysis. Short Time-series Expression Miner (STEM) analysis was used to investigate the expression tendency of ECM proteins in different groups.

2.11. Statistical analysis

All quantitative data were expressed as the means ± standard deviation. Statistical analyses were performed using SPSS® software (Chicago, IL). Statistical significance was determined using a one-way analysis of variance (ANOVA) followed by a post hoc test (Bonferroni). A p value less than 0.05 was considered statistically significant.

3. Results

3.1. Coculture of osteoblasts with fibroblasts enhanced osteogenic differentiation

Osteoblasts and fibroblasts were cocultured directly on tissue culture plates as illustrated in Fig. 1a. Morphology and osteogenic differentiation assay were valued at different time points. Special spatial arrangement in the cocultures was observed on day 2, which was not observed on the first day after cell seeding (Fig. 1b). Fibroblasts were

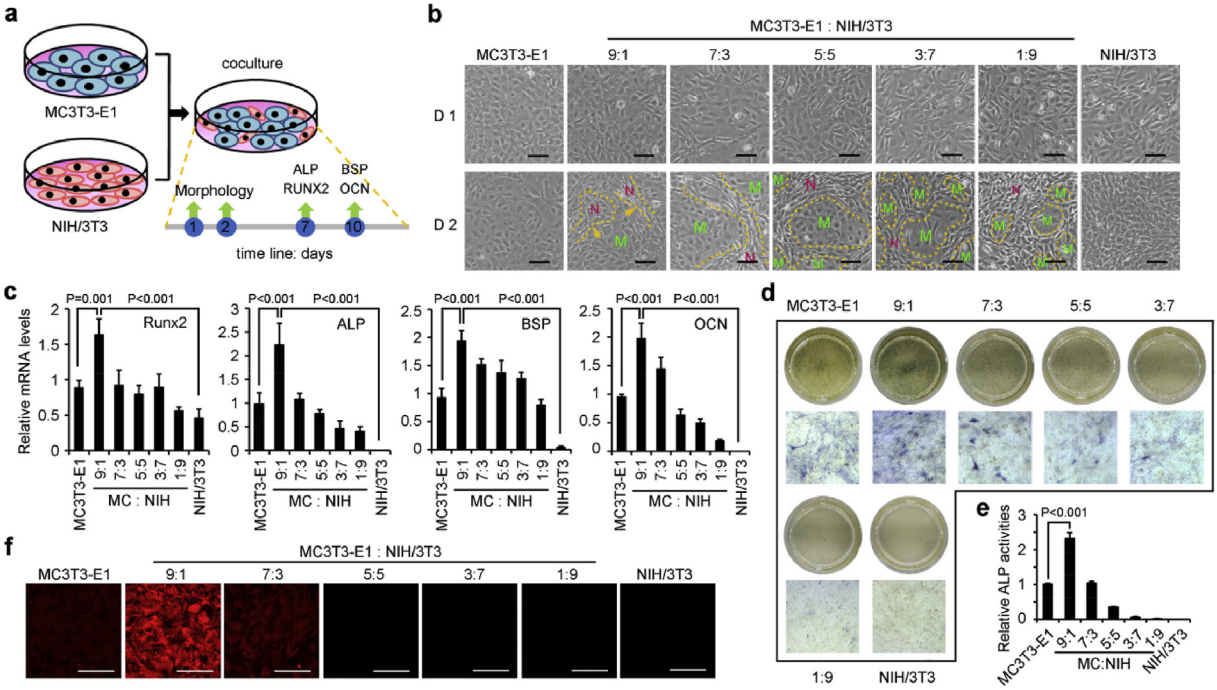

Fig. 1. Coculture of osteoblasts and fibroblasts promoted osteogenic differentiation. (a) Schematic diagram of MC/NIH cocultures. MC3T3-E1 (osteoblasts) and NIH/3T3 (fibroblasts) were cocultured and characterized as time lime shown. (b) Morphology of coculture cells at different ratios was imaged by a phase contrast microscope on day 1 and 2. Green "M" indicated MC3T3-E1 cells; Red "N" indicated NIH/3T3 cells; yellow dotted line indicated the edge between MC3T3-E1 and NIH/3T3 cells. (c) Real-time qPCR analysis of osteogenic associated genes (RUNX2, ALP, BSP and OCN) at different time points as indicated in (a). MC: MC3T3-E1; NIH: NIH/3T3. Protein levels of ALP (blue) and OCN (red) was analyzed by ALP staining (d) and IF staining (f) respectively. The activity of ALP in different groups in 24-well plates was quantified by ImageJ software (e). Images and data are representative of n = 3 individual experiments, and bar heights and error bars were represented as means ± SD. Scale bars: 100 μm (b&e).

presented as vimineous and tended to grow around osteoblast population. Osteoblasts were separated into smaller population along with higher ratio of fibroblasts. Moreover, osteogenic differentiation was also promoted by coculture, especially at the ratio of 9:1 (MC3T3-E1:NIH/3T3, MC/NIH). The expression of RUNX2 and osteogenic markers (ALP, BSP and OCN) was the highest in the MC/NIH (9:1) cells at mRNA levels (Fig. 1c–f). ALP staining was used to analyze the activity of ALP in different groups (Fig. 1d), and quantification of the staining showed the highest activity of ALP in MC/NIH (9:1) cells (Fig. 1e). Consistently, the protein level of OCN was higher in MC/NIH (9:1) cells than other groups (Fig. 1f). Therefore, our later investigation was mainly focused on the coculture of MC3T3-E1 and NIH/3T3 cells at the ratio of 9:1 (MC:NIH), the abbreviation of which was MC/NIH cocultures. However, mineralization was not obvious in all kinds of cell cultures yet (Fig. S1).

3.2. Extracellular vesicles mediate cell-cell communication from fibroblasts to osteoblasts in cocultures

Cell-cell communication is essential for cell arrangement and cellular activities, and contributes specific ECM formation. To further investigate the intercellular communication in MC/NIH cocultures, osteoblasts and fibroblasts were labeled with green fluorescence protein (GFP) and red fluorescence protein (RFP) respectively, following with coculture of labeled cells (Fig. 2a). As shown in Fig. 2b, little fibroblasts were found on the first day, while more fibroblasts were observed and arranged around osteoblast population on day 2 in cocultures, consistent with bright field images (Fig. 1b). Fibroblasts grew much faster than osteoblasts in cocultures with the special arrangement pattern until overgrowth on osteoblasts, and orange cells with both FPs (GFP and RFP) were observed on day 10. However, the appearance of orange cells may be caused by overlapped cells. To avoid the inaccuracy and make sure the FPs expression precisely, the cocultured cells on day 10 were separated into single cells and double positive cells (GFP/RFP) were still visible (Fig. 2c). Moreover, flow cytometric analysis revealed that almost all fibroblasts retained their original red label, while more than half osteoblasts were shifted to become double positive (Fig. 2d& e). The results indicated osteoblasts absorbed RFPs from fibroblasts, which was further determined by transwell assay in Fig. 2f&g. Extracellular vesicles (EVs) with RFPs were secreted by fibroblasts, penetrated through transwell membrane and observed around osteoblasts underlayer (Fig. 2f). Conversely, no EVs with GFPs were observed around fibroblasts underlayer (Fig. 2g). Moreover, double positive cells were observed in GFP-MC3T3-E1 cells underlayer (Fig. S2a), but still not observed in RFP-NIH/3T3 cells underlayer on day 26 (Fig. S2b). Thus, short distance in direct cocultures enhanced cell-cell communication efficiency, compared with long distance in indirect cocultures (transwell coculture).

3.3. Preparation and characterization of MN-ECM

The specific cell arrangement, cell-cell communication and enhancement of osteogenic differentiation in MC/NIH cocultures necessarily affected ECM secretion and organization, which might be better to mimic microenvironment *in vivo* than ECM from single cell type. To demonstrate the hypothesis, ECM from coculture cells or single cell type was obtained via decellularization after 10 days as illustrated by Fig. 3a. During decellularization, N-ECM showed low binding affinity to tissue culture plates and was easier to be washed away than other two kinds of ECMs. After that, the composition and structure of MN-ECM were characterized (Fig. 3b–g). The morphology of MN-ECM was obviously different from M-ECM and N-ECM when scanned by bright field, SEM and AFM (Fig. 3b). Bright field showed most dense structure of MN-ECM but most loose structure of N-ECM, which reflects the difference of refraction index in ECMs. Under the SEM and AFM scanning, M-ECM was dense with rough surface, while N-ECM was flat

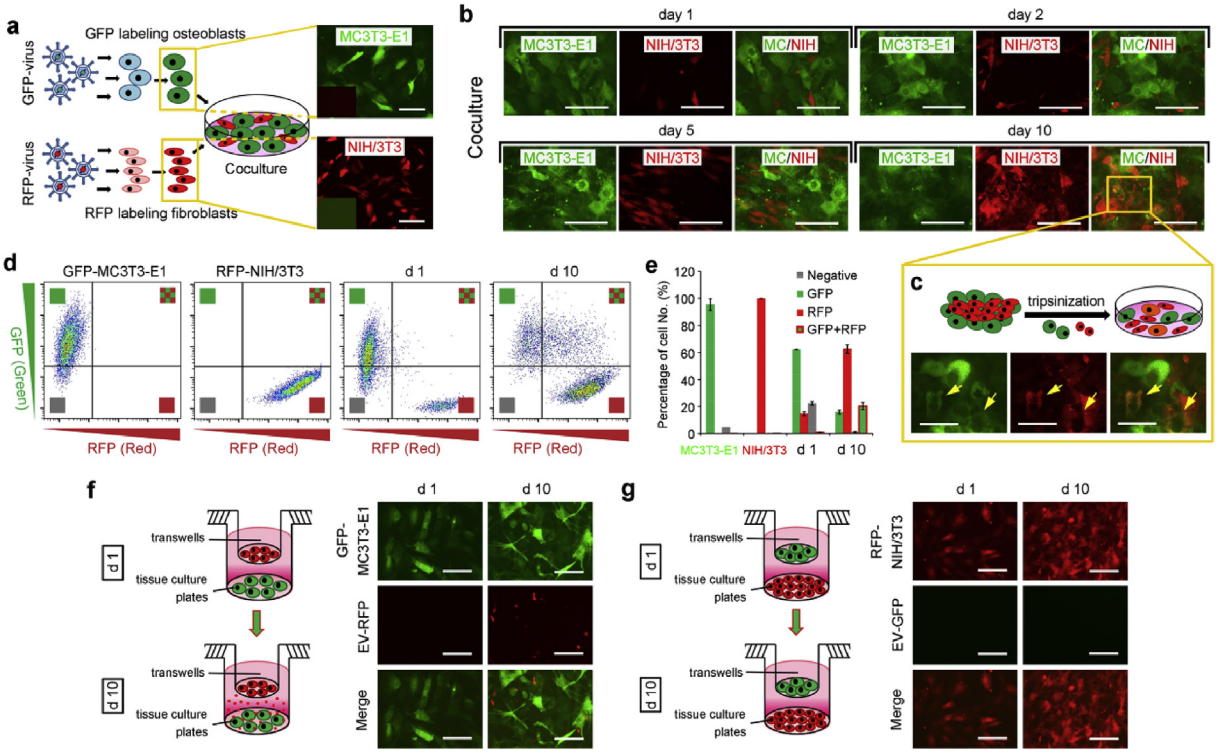

Fig. 2. Extracellular vesicles mediated cell-cell communication from NIH/3T3 to MC3T3-E1. (a) Fluorescence protein labeling of cells via virus transfection. MC3T3-E1 was labeled with GFP, and NIH/3T3 was labeled with RFP. (b) IF images of labeled coculture cells (MC/NIH) under a fluorescence microscope. Green cells were MC3T3-E1 (MC), and red cells were NIH/3T3 (NIH). (c) MC/NIH cocultures were tripsinized into single cells, and were imaged under a fluorescence microscope. Yellow arrows indicated double positive cells. (d–e) Flow cytometry analysis of GFP-MC3T3-E1, RFP-NIH/3T3 and GFP-MC/RFP-NIH cocultures on day 1 and 10. GFP-MC3T3-E1 cells in cocultures on day 10 were smeared, and shifted into double positive area (d), the number of which was ~20% (e). (f–g) GFP-MC3T3-E1 and RFP-NIH/3T3 were cocultured indirectly via transwell system: RFP-NIH/3T3 cells cultured in transwells and GFP-MC3T3-E1 cells cultured on tissue culture plates (f); or GFP-MC3T3-E1 cells cultured in transwells and RFP-NIH/3T3 cells cultured on tissue culture plates (g). Cells on tissue culture plates were imaged. Images and data are representative of n = 3 individual experiments, and bar heights and error bars represent means ± SD. Scale bars: 100 μm.

with little holes. MN-ECM combined and reorganized these two kinds of ECMs. Consistently, the distribution of COL1A1 fibers in MN-ECM also combined dense appearance in M-ECM and loose appearance in N-ECM with a certain organization (Fig. 3c). OCN, an important ECM protein in bone tissue, was not expressed in N-ECM, and the distribution was distinct between M-ECM and MN-ECM. We further quantified total protein content (Fig. 3d) and GAG content (Fig. 3e) in three kinds of ECM. MN-ECM showed the highest level among them. Moreover, the distribution of whole collagen proteins were differed from each other (Fig. 3f) and the collagen content was quantified accordingly (Fig. 3g). The collagens were schistose in M-ECM, while they were loose in N-ECM. In MN-ECM, the collagens were presented as net shape with the highest content. The specific morphology and structure of MN-ECM might be caused by the alteration of cellular activities, which were affected by cell-cell communication in the cocultures.

3.4. Cell behaviors regulated by MN-ECM in vitro

To investigate the guiding effect of coculture ECM on cells in comparison to that of ECM from single cell type, BMSCs and osteoblasts were seeded on M-ECM, MN-ECM and N-ECM respectively and cell behaviors including cell proliferation, cell adhesion and osteogenic differentiation were assessed (Fig. 4a). At first, we assessed the effect of coculture ECM at different ratios (MC:NIH) on cell proliferation (Fig. 4b–c, Fig. S3). Consistent with cell behaviors in coculture system (Fig. 1a), MN-ECM at the ratio of 9:1 showed the best promotion on BMSCs proliferation on day 3 and 5 (Fig. 4b), and on osteoblasts proliferation on day 4 and 7 (Fig. 4c), compared with other ratios and single cell type secreted ECM. Proliferation rate was highest on MN-ECM at 9:1 in both BMSCs and osteoblasts at early and middle stage, but was similar in all groups at a low level at late stage in osteoblasts (Fig. S3a&b). No significant difference was observed in fibroblasts cultured on different ECMs (Fig. S3c). Thus, we also mainly focused on guiding effects of cell behavior on MN-ECM at 9:1 ratio later.

Cell adhesion was assessed by F-actin staining at different time points (1 h, 4 h and 24 h) (Fig. 4d–i). Cells on MN-ECM exhibited specific appearance, which was different from that on other two kinds of ECMs. For BMSCs, much more pseudopodia were apparent in the cells on MN-ECM than those on M-ECM and N-ECM at 4 h (Fig. 4d). By 24 h, the cells on MN-ECM were vimineous, while the cells on M-ECM and N-ECM were spreading (Fig. 4d). Consistently, perimeter of cells on MN-ECM was much longer than that on M-ECM or N-ECM (Fig. 4f), though no significant difference of area was observed between three groups (Fig. 4e). Similar to BMSCs, osteoblasts on MN-ECM also showed a unique appearance which was vimineous at 24 h (Fig. 4g). The difference was that pseudopodia were apparent in osteoblasts on MN-ECM as early as 1 h, which was more than that on N-ECM and not apparent in the cells on M-ECM. Moreover, statistical analysis showed higher area of osteoblasts on MN-ECM at 1 h, and lower area by 4 h and 24 h, compared with M-ECM group (Fig. 4h), while perimeter of cells was longest in MN-ECM group (Fig. 4i).

Mineralization is important for osteogenic differentiation *in vitro* and bone regeneration *in vivo*. Alizarin red S staining was used to assess the mineralization in BMSCs and osteoblasts cultured on different ECMs (Fig. 4j-m). MN-ECM significantly enhanced the mineralization of BMSCs at 2 and 4 weeks (Fig. 4j&k). For osteoblasts, calcium deposition was also the highest in the cells on MN-ECM at 4 weeks, but the mineralization ability of osteoblasts was lower than that of BMSCs (Fig. 4l &m).

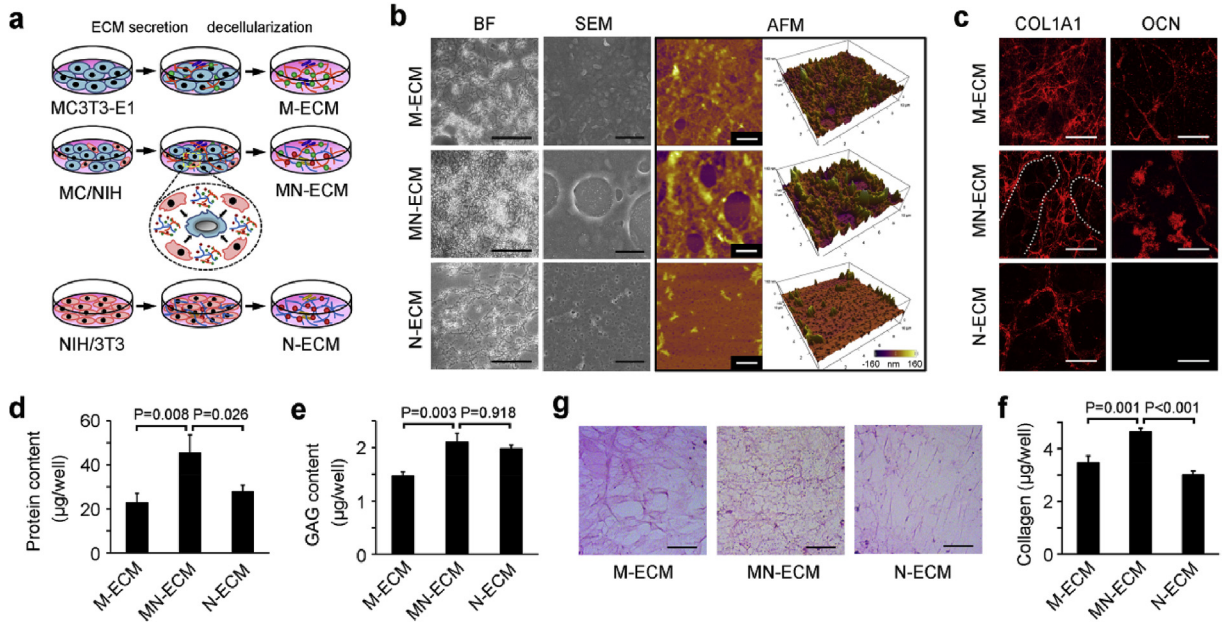

Fig. 3. Generation and characterization of ECM from secreted single cell type or cocultured cells. (a) Schematic diagram of cell-secreted ECM generation. Single cell type (MC3T3-E1 or NIH/3T3) or MC/NIH cocultures were cultured on tissue plates for 10 days to generate ECM. Complicated ECM was secreted by MC/NIH cocultures because of cell-cell communication. Decellularization was introduced to remove cells and ECM was left. (b) ECM morphology was characterized by phase contrast microscope (bright field, BF), scanning electron microscope (SEM) and atomic force microscope (AFM). Scale bars: 50 μm (BF); 2 μm (SEM and AFM). (c) IF staining of COL1A1 and OCN. Scale bars: 20 μm. Both dense and loose collagen fibers were observed in MN-ECM and separated by white dotted line. (d–f) Total protein content (d) and GAG content (e) in ECMs on 24-well plates were assessed. (f–g) Collagen fibers were stained as red (f). Collagen content in ECMs on 24-well plates was quantified according to the instructions of Sirius Red/Fast Green collagen staining kit. Scale bars: 40 μm. Images and data are representative of n = 3 individual experiments, and bar heights and error bars represent means ± SD.

3.5. Bone regeneration promoted by ECM modified scaffolds in vivo

SIS scaffolds were ornamented with M-ECM, MN-ECM and N-ECM *in situ*, and the complex constructs were implanted in a mouse calvarial defect model (Fig. 5a). X-ray analysis showed significant calcifying new bone formation in the middle of the defects with MN-ECM scaffolds implantation (Fig. 5b). Statistical analysis revealed MN-ECM was the most beneficial for calvarial bone regeneration in comparison to the ECMs secreted by single cell type (M-ECM and N-ECM) (Fig. 5c). Histological evaluation with H&E (Fig. 5d) and Masson trichrome staining (MTS) (Fig. 5e) further demonstrated the promotion of MN-ECM in bone repair. The newly formed bone with typical structure as sparse osteocytes embedded in lacunas with osteoblasts lining the outer edge of the bone tissue was observed in all three ECM scaffolds at 6 weeks (Fig. 5d). However, marrow cavities or blood vessels were only presented in the defects with MN-ECM scaffolds (Fig. 5d). Bone formation ratio was also higher after implantation of MN-ECM scaffolds, compared with implantation of M-ECM or N-ECM scaffolds (Fig. 5f). Newly formed collagenous fibers in MN-ECM scaffolds were much more than that in M-ECM and N-ECM scaffolds at 3 weeks (Fig. 5e&g). By 6 weeks, newly formed collagenous fibers were observed in all kinds of ECMs (M-ECM, MN-ECM and N-ECM) (Fig. 5e). Consistent with H&E staining, marrow cavities or blood vessels were apparent in the defects with MN-ECM scaffolds (Fig. 5e). The results indicated MN-ECM provided the most suitable microenvironment to mimic bone tissue niche for bone regeneration *in vivo*.

3.6. ECM secreted by MC/NIH cocultures displayed a specific matrisome signature

To investigate the molecular mechanism of the generated complex ECM in coculture system (MN-ECM), the protein composition in ECMs was comprehensively characterized by proteomic analysis (Fig. 6). Quantitative proteomic approaches by labeling TMT was performed to evaluate the relative abundance of ECM proteins among three kinds of ECMs. Total 178 ECM proteins were identified, of which 80 proteins were core matrisome proteins and 98 proteins were matrisome-associated proteins (Fig. 6a). Though the number of core matrisome proteins was less than 50%, the protein abundance (PSMs) of these proteins was more than 80%. In addition to the core matrisome proteins, the ECMs served as a reservoir for regulators, secreted factors and other ECM-affiliated proteins were less abundant but with more kinds of proteins. Statistical analysis showed 124 proteins were assessed with significant difference among three kinds of ECMs (M-ECM, MN-ECM and N-ECM) (Fig. 6b).

The expression of ECM proteins was presented in the format of a heat map (Fig. 6c), and short time-series expression miner (STEM) was introduced to analyze the results (Fig. 6d). In the present study, the ECM proteins were separated into four clusters according to their expression tendency. Sixty-two proteins were expressed highest in M-ECM with major core matrisome proteins (cluster 1), while only 19 proteins were expressed highest in N-ECM with major matrisome-associated proteins (cluster 4). Interestingly, 28 proteins were assessed as highest expression (cluster 2) and 12 proteins were assessed as lowest expression (cluster 3) in MN-ECM. The STEM in each sub-category of ECM proteins was also presented and each ECM protein was listed (Figs. S4–S9). The ratio of proteins in cluster 2 was higher in collagens, proteoglycans, regulators, affiliated proteins and secreted factors than the ratio of that in total proteins, only except glycoproteins (Fig. S10). To further define the specific protein composition in MN-ECM, the fold change of ECM proteins in cluster 2 and cluster 3 was listed from high to low in Fig. 6e&f respectively. The top 17 ECM proteins expressed highest in MN-ECM were mainly matrisome-associated proteins, besides 3 core matrisome proteins (VTN, DCN and COL24A1). The results indicated core matrisome proteins mainly depended on cell type, and the expression of these proteins tended to be stable relatively without great changes. The function of MN-ECM might be mainly regulated by matrisome-associated proteins.

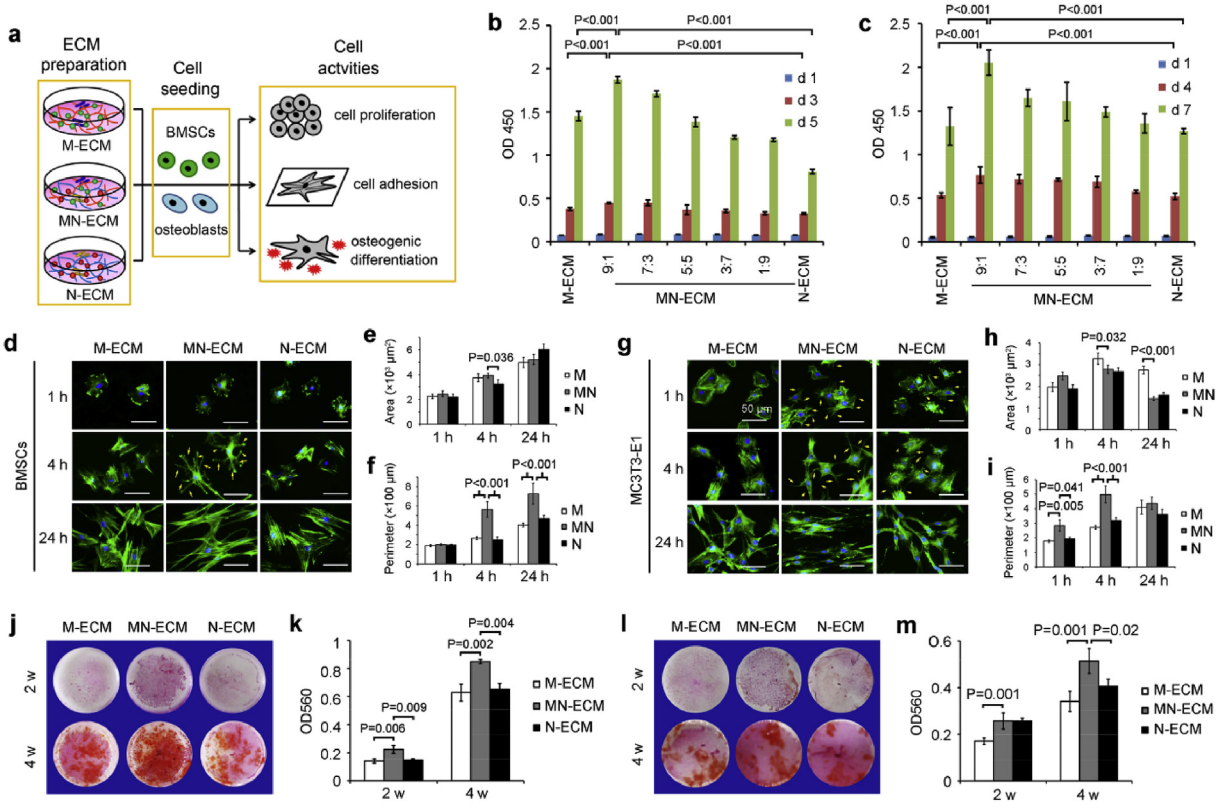

Fig. 4. Bone mimetic ECM engineered by cocultured cells facilitated cell proliferation, adhesion and osteogenic differentiation. (a) Schematic diagram of cellular guiding effects of ECM on cell proliferation, adhesion and osteogenic differentiation. M-ECM, MN-ECM and N-ECM were prepared, following with seeding of BMSCs and osteoblasts to assess the effects. (b–c) MN-ECM promoted cell proliferation of BMSCs (b) and MC3T3-E1 (c), especially at the ratio of 9:1 (MC:NIH) (n = 6). (d–i) Cell spreading morphology of BMSCs (d–f) and MC3T3-E1 (g–i) on MN-ECM (9:1) was unique. F-actin of BMSCs (d) and MC3T3-E1 (g) was stained by FITC-phalloidin. Representative images were shown. Scale bars represented 50 μm. Cell area (e&h) and cell perimeter (f&i) were calculated based on images by ImageJ software. Twenty cells (n = 20) were measured for each individual samples and four individual experiments (n = 4) were performed for each group. (j–m) MN-ECM (9:1) promoted osteogenic mineralization of BMSCs (j&k) (n = 3) and MC3T3-E1 (l&m) (n = 4). BMSCs were cultured in osteogenic induction medium (100 nM dexamethazone, 50 μg/ml ascorbic acid and 10 mM β-glycerophosphate). Mineralization was stained by Alizarin red S and captured by a camera (j&l). The stained dye was extracted with cetylpyridinium chloride and measured at 560 nm (k&m).

GO analysis of proteins in cluster 2 and 3 suggested MN-ECM might contribute to multiple biological process of cells (including biological adhesion, cell proliferation, cell differentiation, cell migration, angiogenesis and immune system) (Fig. 6g, Table S1&S2) and molecular functions (including protein binding, iron binding and ECM binding) (Fig. 6h, Table S3&S4). Moreover, 15 ECM proteins in cluster 2 and 3 were specifically associated with calcium iron binding among iron binding, which might contribute to osteogenic mineralization (Table S3 &S4).

4. Discussion

Accumulated researches introduced ECM-like scaffolds with tissue mimetic niches for tissue regeneration via recruitment of endogenous cells [2,38]. Compared with artificial ECM with single or a few compositions, natural ECM secreted by cells harbored a complex network including collagen fibers, glycoproteins, cytokines and proteoglycans under ordered arrangement, and contributed the process. Here, we cocultured fibroblasts and osteoblasts to generate a complex ECM under guidance of unique cell arrangement and cell-cell communication (Figs. 1–4), which effectively regulated proliferation, attachment and osteogenic differentiation of BMSCs and osteoblasts *in vitro* (Fig. 5), and enhanced bone regeneration *in vivo* (Fig. 6). The complex ECM generated in a coculture system represents several unique advantages: (1) better guidance of multiple cell arrangement than single cell culture; (2) tissue mimetic niche organized by multiple cells under cell-cell communication; (3) easy operability and controllability with low immunogenicity after implantation *in vivo*; (4) extensive application with different cell composition depended on tissue properties and (5) surface modification on multiple biomaterials as “off-shelf” implants after decellularization.

Tissues are composed of ECM with mechanical and physiological support, and multiple cells with accurate organization. The arrangement of different cells is essential for tissue ECM generation with unique microenvironment. In the present study, fibroblasts and osteoblasts were cocultured together and unique cell arrangement was formed along with alteration of cellular activities (Fig. 1). In the coculture system, fibroblasts grew fast around osteoblasts and osteogenic maturation of osteoblasts was stimulated by surrounding fibroblasts due to the specific cell order and cell-cell communication. Previously, a gold standard coculture model was tranwell culture. The model was beneficial to investigate paracrine pathways between different cells, but blocked cell interaction and cell arrangement which limited application in tissue regeneration. Later studies ever did efforts to arrange different cells together in a specific order artificially. For example, HUVEC and MSCs were mixed into fibrin bioinks and printed HUVEC fibers and MSCs fibers alternately in a round shape [26]. Here, we found fibroblasts and osteoblasts could form circle-surrounding construct spontaneously via their own activities which should be closer to clarify cell-cell communication naturally. Accordingly, recent studies introduced coculture of multiple cells direct together to mimic tissues *in vivo* [27,39,40]. Myoblasts were cocultured with hMSCs to induce trans-differentiation under electric field stimulation [27]. Coculture of glioblastoma cells and endothelial cells mimicked tumor niche to increase

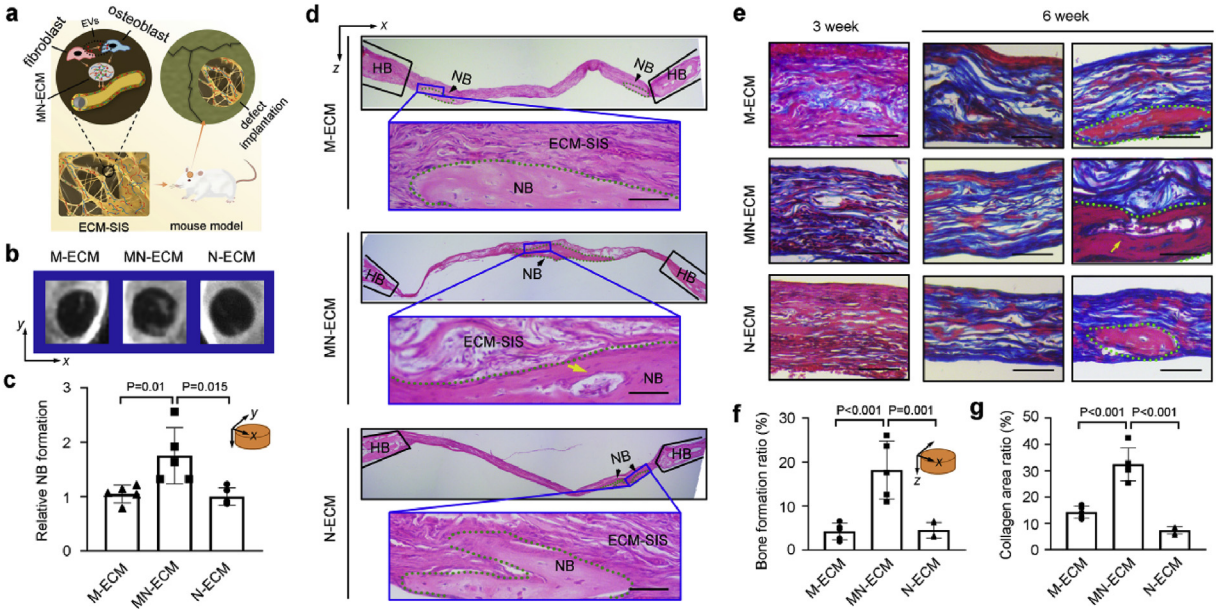

Fig. 5. Bone mimetic ECM engineered by cocultured cells enhanced bone regeneration *in vivo*. (a) Schematic diagram of ECM ornamented SIS scaffolds implanted into mouse cavarial defects (Φ = 4 mm). The tissues with defects were collected after 3 or 6 weeks. (b–c) X-ray images of defects implanted with ECM-SIS scaffolds (M-ECM, MN-ECM and N-ECM) (n = 5) at 6 weeks (b). The relative new bone formation was calculated by normalization to new bone formation area in the defects with M-ECM scaffolds at 6 weeks, which was measured by ImageJ software (n = 5) (c). (d) H&E staining of the cross-sections to show the histological morphology of the regenerated defects at 6 weeks. Green dotted region represented newly formed bone (NB) (black arrow). The blue boxes were magnified to present the details of NB. HB: host bone; yellow arrow: marrow cavity. (e) MTS staining of the cross-sections of the regenerated defects at 3 and 6 weeks. Newly formed collagens were visualized as blue and newly formed mature bones were visualized as red. (f) Bone formation ratio was measured by ImageJ software based on H&E staining of cross-sections of the defects at 6 weeks. Sections with newly formed bone were measured for each mouse and 5 mice were analyzed for each group. (g) Collagen area with blue color and the whole scaffold area were measured by ImageJ staining, and the ratio was calculated. Five random fields were measured for each mouse and 5 mice were analyzed for each group. Scale bars represented 50 μm.

glioblastoma cell proliferation and to decrease endothelial cell expression of cell adhesion proteins [39].

The advantage of coculture *in vitro* is convenient to regulate the cell ratio to achieve the best effects. In this study, we designed multiple ratios of osteoblasts and fibroblasts, and 9:1 (MC:MIH) of the seeding ratio was demonstrated to be the best with the highest expression of osteogenic differentiation markers. The advantage of coculture *in vitro* is convenient to regulate the cell ratio to achieve the best effects. In this study, we designed multiple ratios of osteoblasts and fibroblasts, and 9:1 (MC:MIH) of the seeding ratio was demonstrated to be the best with the highest expression of osteogenic differentiation markers. In the cocultures, osteoblasts and fibroblasts were undergoing different cell fates. Osteoblasts were mainly undergoing osteogenic differentiation, along with up-regulation of differentiation markers and alteration of cell morphology (Figs. 1 and 2b). However, proliferation of osteoblasts was inhibited at the meantime. Then, fibroblasts in the cocultures were mainly undergoing cell proliferation (Fig. 2). The cellular activities of osteoblasts and fibroblasts during the coculturing led to the ratio alteration as the higher ratio of fibroblats and lower ratio of osteoblasts on day 10 (Fig. 2d&e). Even though, the seeding ratio of 9:1 (M:N) was demonstrated with the highest activities of osteogenic differentiation (Fig. 1) and the derived ECM was considered as the best for cell proliferation (Fig. 5b&c).There are two possibilities: (1) A small amount of fibroblasts at the beginning is important to trigger the activities of osteoblasts. Then, the proliferation of fibroblasts and cell-cell communications further promotes the events. (2) Osteoblasts secrete the major functional ECM proteins for bone regeneration. Higher amount of fibroblasts diluted the roles of osteoblasts. Proper ratios of osteoblasts and fibroblasts are essential for the functions of the cocultures.

In the MC/NIH coculture system, it's interesting to find that the cell-cell communication was not bi-directional, but mainly unidirectional from fibroblasts to osteoblasts via EVs (Fig. 2). Double staining cells mainly shifted from GFP-osteoblasts after absorbing RFP secreted by fibroblasts. Transwell coculture demonstrated EVs as messengers from fibroblasts to osteoblasts. However, the communication was much slower than coculture together (Fig. S2), which indicated other interactions occurred between the two cell types. It's common that cell-cell communication is the key for higher-order biological functions in multicellular tissues [41,42]. Coculture system provides the opportunity to study the mechanisms of cell-cell communication and multicellular behaviors. In coculture system, cell fate in recipient cells was directed by the cell-cell communication to support a differentiated function, including paracrine, exosomes or EVs, and direct cell-cell interactions via transmembrane proteins [41]. Consistent with our study, juvenile chondrocytes (CHs) in coculture with adult mesenchymal stem cells (MSCs) improved chondrogenesis of MSCs via EVs from CHs to MSCs and promoted cartilage engineering [25].

Our previous studies focused on the effects of single cell type behavior on ECM secretion and ECM-ornemented biomaterials for bone regeneration [34–36]. Compared with ECM from single cell type, ECM from multiple cells presented multiple advantages due to multiple cell organization and cell-cell communication mentioned above. Cumulative evidences have demonstrated the interactions between two cell types improved ECM remodeling [25,43]. ECM providing complex local heterogeneous microenvironments modulated cellular activities via cell-matrix interactions [44,45]. The composition and structure of ECM depended on cell type, local environment, availability of substrates and shear forces [46,47]. Spatial, chemical and mechanical cues in ECM influenced cell-ECM interactions via activation of intracellular signaling cascades and further affected cellular behaviors [48]. Consistently, our present study demonstrated the ECM generated by MC/NIH cocultures possessed unique structure and molecular composition (Figs. 3 and 4) and was beneficial for cell proliferation, adhesion and osteogenic differentiation (Fig. 5), and further promoted bone regeneration *in vivo* (Fig. 6).

Though ECM has been realized as a functional biomaterial with

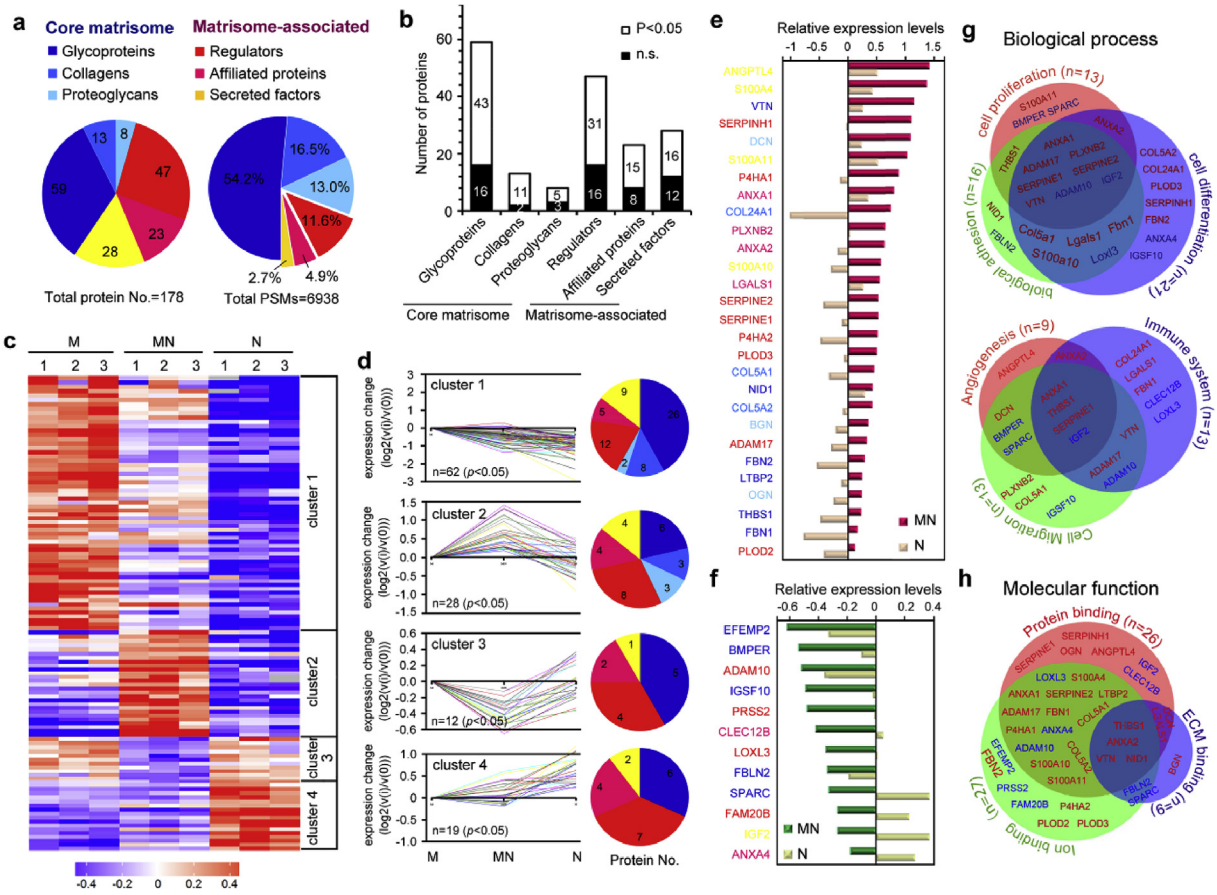

Fig. 6. Quantitative proteomic analysis of ECMs secreted by cocultured cells (MN-ECM) revealed a unique matrisome signature. (a) Matrisome signature of cell secreted ECM as presented by pie chart. Distribution of ECM proteins was calculated by protein numbers (left) and protein abundance (PSMs, right) of each matrisome protein sub-category, respectively. (b) Distribution of protein numbers with or without statistical significance among three kinds of ECM. (c) Heatmap of quantitative proteomics using TMT labeling. The fold-change in protein detection levels normalized to the mean of M-ECM in $\log_2$ scale was shown. (d) Short-time series expression miner (STEM) of ECM proteins with statistical significance. According to the expression tendency, ECM proteins were divided into four clusters. Distribution of protein numbers was presented for each cluster. (e–f) ECM proteins in cluster 2 (e) and cluster 3 (f) were listed from highest changes to lowest changes. The color of proteins was consistent with the sub-category in pie chart. (g–h) GO analysis of ECM proteins in cluster 2 and cluster 3, including biological process (g) and molecular function (h). Red color represents the ECM proteins expressed highest in MN-ECM in cluster 2 and blue color represents the proteins expressed lowest in MN-ECM in cluster 3. Triplicate independent experiments were performed for each group.

various biochemical components to recapitulate complicated microenvironments and broadly applied for tissue regeneration [49,50], the further question was why they worked in specificity. Many efforts have been made to rationalize the specific functionalities of ECM biomaterials, including proteomic analysis [51–53]. Proteomic analysis provided a powerful way to understand ECM matrisome comprehensively, including the compositions and potential biological functions [54,55]. Proteomic composition of stem cell-derived ECM has been characterized, including ECM from bone-marrow-derived MSC [54], adipose-derived MSC [54] and osteoblast-differentiated MSCs [56]. However, proteomic composition of ECM from fibroblasts or osteoblasts, especially cocultured cells, was rarely reported. Here, we figured out unique ECM matrisome from MC/NIH cocultures and single cell type (fibroblasts or osteoblasts) respectively via proteomic analysis. It's interesting that the levels of ECM proteins in MN-ECM were not only between M-ECM and N-ECM, but with great change. In MN-ECM, 28 proteins were expressed highest and 12 proteins were expressed lowest. The results might be caused by the activity alteration of osteoblasts, which was guided by fibroblast in the cocultures (Fig. 2). The most abundance of ECM proteins in N-ECM were matrisome-associated proteins. Consistently, fibroblasts greatly increased matrisome-associated protein secretion of osteoblasts in the cocultures (Fig. 6e), including ANGPTL4, S100A4, SERPINH1, S100A11 and so on (from high to low). These genes were reported to play essential roles in biological process and might contribute to the function of MN-ECM. For example, ANGPTL4 was a key factor in the modulation of angiogenesis and in bone regeneration [57]. The expression of ANGPTL4 was increased in mineralizing periodontal cells on day 14 of culture and was induced by hypoxia in periodontal fibroblasts [58]. SERPINH1 encodes the collagen chaperone HSP47 that binds to the type I precollagen trimers and regulated the folding and stabilization of triple helical domain. *SERPINH1* mutations have been associated with osteogenesis imperfect [59]. Thus, the results also provided orientations to investigate ECM matrisome in depth in future.

5. Conclusions

In conclusion, the present study developed a novel strategy to generate tissue mimetic ECM with excellent bioactivities for bone regeneration. In the coculture system, existence of fibroblasts promoted osteoblasts undergoing osteogenic maturation. The cell communication between different cell types guided the tissue mimetic ECM engineering with specific morphology and molecular components. The generated ECM from coculture cells provided unique biophysical and biochemical cues for cell-matrix interactions and regulated cell behaviors. Furthermore, the complicated ECM ornamented scaffolds with suitable microenvironment promoted collagen regeneration and new bone formation, which might be caused by the recruitment of endogenous cells

and stimulation of self-healing process. The “off-shelf” products with higher bioactivities in ECM from multiple cell types than that from single cell type should be a bright choice for biomaterial decoration for tissue engineering and regenerative medicine.

Funding

This work was supported by the National Natural Science Foundation of China (Grant No. 31300800 and 81702625), the Zhejiang Province Welfare Technology Application Research Project (Grant No. 2017C33135), the Natural Science Foundation of Ningbo (Grant No. 2018A610202 and 2019A610309) and the K.C. Wong Magna Fund in Ningbo University.

CRediT authorship contribution statement

Mei Li: Formal analysis, Data curation, Writing - original draft. **Anqi Zhang:** Investigation. **Jiajing Li:** Investigation. **Jing Zhou:** Formal analysis. **Yanan Zheng:** Formal analysis. **Chi Zhang:** Formal analysis. **Dongdong Xia:** Formal analysis. **Haijiao Mao:** Formal analysis. **Jiyuan Zhao:** Formal analysis, Data curation, Writing - original draft.

Declaration of competing interest

The authors declara that they have no known competing financial interests or personal relationships that could have appaered influence the work reported in the papaer.

Appendix A. Supplementary data

Supplementary data to this article can be found online at https://doi.org/10.1016/j.bioactmat.2020.06.017.

References

[1] K. Sadtler, A. Singh, M.T. Wolf, X.K. Wang, D.M. Pardoll, J.H. Elisseeff, Design, clinical translation and immunological response of biomaterials in regenerative medicine, Nat. Rev. Mater. 1 (7) (2016) 1–17, https://doi.org/10.1038/natrevmats.2016.40.

[2] H.M. Xia, X. Li, W.W. Gao, X. Fu, R.H. Fang, L.F. Zhang, K. Zhang, Tissue repair and regeneration with endogenous stem cells, Nat. Rev. Mater. 3 (7) (2018) 174–193, https://doi.org/10.1038/s41578-018-0027-6.

[3] M. Zhu, W. Li, X. Dong, X. Yuan, A.C. Midgley, H. Chang, Y. Wang, H. Wang, K. Wang, P.X. Ma, H. Wang, D. Kong, In vivo engineered extracellular matrix scaffolds with instructive niches for oriented tissue regeneration, Nat. Commun. 10 (1) (2019) 4620, https://doi.org/10.1038/s41467-019-12545-3.

[4] L. Moroni, J.A. Burdick, C. Highley, S.J. Lee, Y. Morimoto, S. Takeuchi, J.J. Yoo, Biofabrication strategies for 3D in vitro models and regenerative medicine (vol 3, pg 21, 2018), Nat. Rev. Mater. 3 (5) (2018) 21–37, https://doi.org/10.1038/s41578-018-0020-01.

[5] A.E. Stanton, X. Tong, F. Yang, Extracellular matrix type modulates mechanotransduction of stem cells, Acta Biomater. 96 (2019) 310–320, https://doi.org/10.1016/j.actbio.2019.06.048.

[6] G.Y. Huang, F. Li, X. Zhao, Y.F. Ma, Y.H. Li, M. Lin, G.R. Jin, T.J. Lu, G.M. Genin, F. Xu, Functional and biomimetic materials for engineering of the three-dimensional cell microenvironment, Chem. Rev. 117 (20) (2017) 12764–12850, https://doi.org/10.1021/acs.chemrev.7b00094.

[7] Z.K. Cui, S. Kim, J.J. Baljon, B.M. Wu, T. Aghaloo, M. Lee, Microporous methacrylated glycol chitosan-montmorillonite nanocomposite hydrogel for bone tissue engineering, Nat. Commun. 10 (1) (2019) 3523, https://doi.org/10.1038/s41467-019-11511-3.

[8] A.M. Rosales, K.S. Anseth, The design of reversible hydrogels to capture extracellular matrix dynamics, Nat. Rev. Mater. 1 (2) (2016) 15012, https://doi.org/10.1038/natrevmats.2015.12 ARTN 15012.

[9] M.R. Lutolf, F.E. Weber, H.G. Schmoekel, J.C. Schense, T. Kohler, R. Muller, J.A. Hubbell, Repair of bone defects using synthetic mimetics of collagenous extracellular matrices, Nat. Biotechnol. 21 (5) (2003) 513–518, https://doi.org/10.1038/nbt818.

[10] L.T.A. Hong, Y.M. Kim, H.H. Park, D.H. Hwang, Y. Cui, E.M. Lee, S. Yahn, J.K. Lee, S.C. Song, B.G. Kim, An injectable hydrogel enhances tissue repair after spinal cord injury by promoting extracellular matrix remodeling, Nat. Commun. 8 (2017), https://doi.org/10.1038/s41467-017-00583-8 ARTN 533.

[11] E.S. Place, N.D. Evans, M.M. Stevens, Complexity in biomaterials for tissue engineering, Nat. Mater. 8 (6) (2009) 457–470, https://doi.org/10.1038/Nmat2441.

[12] G.S. Hussey, J.L. Dziki, S.F. Badylak, Extracellular matrix-based materials for regenerative medicine, Nat. Rev. Mater. 3 (7) (2018) 159–173, https://doi.org/10.1038/s41578-018-0023-x.

[13] G.G. Giobbe, C. Crowley, C. Luni, S. Campinoti, M. Khedr, K. Kretzschmar, M.M. De Santis, E. Zambaiti, F. Michielin, L. Meran, Q. Hu, G. van Son, L. Urbani, A. Manfredi, M. Giomo, S. Eaton, D. Cacchiarelli, V.S.W. Li, H. Clevers, P. Bonfanti, N. Elvassore, P. De Coppi, Extracellular matrix hydrogel derived from decellularized tissues enables endodermal organoid culture, Nat. Commun. 10 (1) (2019) 5658–5671, https://doi.org/10.1038/s41467-019-13605-4.

[14] Q. Xing, Z.C. Qian, W.K. Jia, A. Ghosh, M. Tahtinen, F. Zhao, Natural extracellular matrix for cellular and tissue biomanufacturing, ACS Biomater. Sci. Eng. 3 (8) (2017) 1462–1476, https://doi.org/10.1021/acsbiomaterials.6b00235.

[15] J. Madhusoodanan, Matrix mimics shape cell studies, Nature 566 (7745) (2019) 563–565, https://doi.org/10.1038/d41586-019-00681-1.

[16] U.H. Langen, M.E. Pitulescu, J.M. Kim, R. Enriquez-Gasca, K.K. Sivaraj, A.P. Kusumbe, A. Singh, J. Di Russo, M.G. Bixel, B. Zhou, L. Sorokin, J.M. Vaquerizas, R.H. Adams, Cell-matrix signals specify bone endothelial cells during developmental osteogenesis, Nat. Cell Biol. 19 (3) (2017) 189–201, https://doi.org/10.1038/ncb3476.

[17] C.J. Li, G.H. Zhen, Y. Chai, L. Xie, J.L. Crane, E. Farber, C.R. Farber, X.H. Luo, P.S. Gao, X. Cao, M. Wan, RhoA determines lineage fate of mesenchymal stem cells by modulating CTGF-VEGF complex in extracellular matrix, Nat. Commun. 7 (2016) 11455, https://doi.org/10.1038/ncomms11455 ARTN 11455.

[18] M.C. Prewitz, S.F. Philipp, V.B. Malte, F. Jens, S.E. Aline, N. Christian, M. Katrin, A. Konstantinos, W. Claudia, H. Bernard, Tightly anchored tissue-mimetic matrices as instructive stem cell microenvironments, Nat. Methods 10 (8) (2013) 788–794, https://doi.org/10.1038/nmeth.2523.

[19] M. Li, T. Zhang, J. Jiang, Y. Mao, A. Zhang, J. Zhao, ECM coating modification generated by optimized decellularization process improves functional behavior of BMSCs, Materials science & engineering, Mater. Biol. Appl. 105 (2019) 110039, , https://doi.org/10.1016/j.msec.2019.110039.

[20] S. Toda, L.R. Blauch, S.K.Y. Tang, L. Morsut, W.A. Lim, Programming self-organizing multicellular structures with synthetic cell-cell signaling, Science 361 (6398) (2018) 156–162, https://doi.org/10.1126/science.aat0271.

[21] L.A. Johnston, Competitive interactions between cells: death, growth, and geography, Science 324 (5935) (2009) 1679–1682, https://doi.org/10.1126/science.1163862.

[22] J.H. Lee, D.H. Bhang, A. Beede, T.L. Huang, B.R. Stripp, K.D. Bloch, A.J. Wagers, Y.H. Tseng, S. Ryeom, C.F. Kim, Lung stem cell differentiation in mice directed by endothelial cells via a BMP4-NFATc1-thrombospondin-1 Axis, Cell 156 (3) (2014) 440–455, https://doi.org/10.1016/j.cell.2013.12.039.

[23] J.A. Zepp, W.J. Zacharias, D.B. Frank, C.A. Cavanaugh, S. Zhou, M.P. Morley, E.E. Morrisey, Distinct mesenchymal lineages and niches promote epithelial self-renewal and myofibrogenesis in the lung, Cell 170 (6) (2017) 1134–1148, https://doi.org/10.1016/j.cell.2017.07.034.

[24] X. Zhang, C.A. Simmons, J. Paul Santerre, Paracrine signalling from monocytes enables desirable extracellular matrix accumulation and temporally appropriate phenotype of vascular smooth muscle cell-like cells derived from adipose stromal cells, Acta Biomater. 103 (2020) 129–141, https://doi.org/10.1016/j.actbio.2019.12.006.

[25] M. Kim, D.R. Steinberg, J.A. Burdick, R.L. Mauck, Extracellular vesicles mediate improved functional outcomes in engineered cartilage produced from MSC/chondrocyte cocultures, Proc. Natl. Acad. Sci. U. S. A. 116 (5) (2019) 1569–1578, https://doi.org/10.1073/pnas.1815447116.

[26] C. Piard, A. Jeyaram, Y. Liu, J. Caccamese, S.M. Jay, Y. Chen, J. Fisher, 3D printed HUVECs/MSCs cocultures impact cellular interactions and angiogenesis depending on cell-cell distance, Biomaterials 222 (2019) 119423, , https://doi.org/10.1016/j.biomaterials.2019.119423.

[27] S. Naskar, V. Kumaran, Y.S. Markandeya, B. Mehta, B. Basu, Neurogenesis-on-Chip: electric field modulated transdifferentiation of human mesenchymal stem cell and mouse muscle precursor cell coculture, Biomaterials 226 (2020) 119522, , https://doi.org/10.1016/j.biomaterials.2019.119522.

[28] Y.V. Shih, S. Varghese, Tissue engineered bone mimetics to study bone disorders ex vivo: role of bioinspired materials, Biomaterials 198 (2019) 107–121, https://doi.org/10.1016/j.biomaterials.2018.06.005.

[29] H.C. Blair, Q.C. Larrouture, Y. Li, H. Lin, D. Beer-Stoltz, L. Liu, R.S. Tuan, L.J. Robinson, P.H. Schlesinger, D.J. Nelson, Osteoblast differentiation and bone matrix formation in vivo and in vitro, Tissue Eng. B Rev. 23 (3) (2017) 268–280, https://doi.org/10.1089/ten.TEB.2016.0454.

[30] I.G. Kim, M.P. Hwang, P. Du, J. Ko, C.W. Ha, S.H. Do, K. Park, Bioactive cell-derived matrices combined with polymer mesh scaffold for osteogenesis and bone healing, Biomaterials 50 (2015) 75–86, https://doi.org/10.1016/j.biomaterials.2015.01.054.

[31] M. Li, C. Zhang, X. Li, Z. Lv, Y. Chen, J. Zhao, Isoquercitrin promotes the osteogenic differentiation of osteoblasts and BMSCs via the RUNX2 or BMP pathway, Connect. Tissue Res. (2018) 1–11, https://doi.org/10.1080/03008207.2018.1483358.

[32] M. Li, C. Zhang, M. Cheng, Q. Gu, J. Zhao, Small intestinal submucosa: a potential osteoconductive and osteoinductive biomaterial for bone tissue engineering, Mater. Sci. Eng. Mater. Biol. Appl. 75 (2017) 149–156, https://doi.org/10.1016/j.msec.2017.02.042.

[33] M. Li, Q. Gu, M. Chen, C. Zhang, S. Chen, J. Zhao, Controlled delivery of icariin on small intestine submucosa for bone tissue engineering, Mater. Sci. Eng. Mater. Biol. Appl. 71 (2017) 260–267, https://doi.org/10.1016/j.msec.2016.10.016.

[34] C. Zhang, M. Li, J. Zhu, F. Luo, J. Zhao, Enhanced bone repair induced by human

adipose-derived stem cells on osteogenic ECM ornamented small intestinal submucosa, Regen. Med. 12 (5) (2017) 541–552, https://doi.org/10.2217/rme-2017-0024.
[35] M. Li, C. Zhang, Y. Mao, Y. Zhong, J. Zhao, A cell-engineered small intestinal submucosa-based bone mimetic construct for bone regeneration, Tissue Eng. 24 (13-14) (2018) 1099–1111, https://doi.org/10.1089/ten.TEA.2017.0407.
[36] M. Li, C. Zhang, Y. Zhong, J. Zhao, A novel approach to utilize icariin as icariin-derived ECM on small intestinal submucosa scaffold for bone repair, Ann. Biomed. Eng. 45 (11) (2017) 2673–2682, https://doi.org/10.1007/s10439-017-1900-y.
[37] J.R. Wisniewski, A. Zougman, N. Nagaraj, M. Mann, Universal sample preparation method for proteome analysis, Nat. Methods 6 (5) (2009) 359–362, https://doi.org/10.1038/nmeth.1322.
[38] F.D. Miller, D.R. Kaplan, Mobilizing endogenous stem cells for repair and regeneration: are we there yet? Cell. Strm. Cell. 10 (6) (2012) 650–652, https://doi.org/10.1016/j.stem.2012.05.004.
[39] C. Wang, J. Li, S. Sinha, A. Peterson, G.A. Grant, F. Yang, Mimicking brain tumor-vasculature microanatomical architecture via co-culture of brain tumor and endothelial cells in 3D hydrogels, Biomaterials 202 (2019) 35–44, https://doi.org/10.1016/j.biomaterials.2019.02.024.
[40] T.H. Qazi, D.J. Mooney, G.N. Duda, S. Geissler, Biomaterials that promote cell-cell interactions enhance the paracrine function of MSCs, Biomaterials 140 (2017) 103–114, https://doi.org/10.1016/j.biomaterials.2017.06.019.
[41] S. Toda, N.W. Frankel, W.A. Lim, Engineering cell-cell communication networks: programming multicellular behaviors, Curr. Opin. Chem. Biol. 52 (2019) 31–38, https://doi.org/10.1016/j.cbpa.2019.04.020.
[42] L. Sapir, S. Tzlil, Talking over the extracellular matrix: how do cells communicate mechanically? Semin. Cell Dev. Biol. 71 (2017) 99–105, https://doi.org/10.1016/j.semcdb.2017.06.010.
[43] C.D. Cook, A.S. Hill, M. Guo, L. Stockdale, J.P. Papps, K.B. Isaacson, D.A. Lauffenburger, L.G. Griffith, Local remodeling of synthetic extracellular matrix microenvironments by co-cultured endometrial epithelial and stromal cells enables long-term dynamic physiological function, Integr. Biol. Quantitat. Biosci. Nano. Macro 9 (4) (2017) 271–289, https://doi.org/10.1039/c6ib00245e.
[44] M. Uroz, S. Wistorf, X. Serra-Picamal, V. Conte, M. Sales-Pardo, P. Roca-Cusachs, R. Guimera, X. Trepat, Regulation of cell cycle progression by cell-cell and cell-matrix forces, Nat. Cell Biol. 20 (6) (2018) 646–654, https://doi.org/10.1038/s41556-018-0107-2.
[45] H. Koo, K.M. Yamada, Dynamic cell-matrix interactions modulate microbial biofilm and tissue 3D microenvironments, Curr. Opin. Cell Biol. 42 (2016) 102–112, https://doi.org/10.1016/j.ceb.2016.05.005.
[46] E.E. Mann, D.J. Wozniak, Pseudomonas biofilm matrix composition and niche biology, FEMS Microbiol. Rev. 36 (4) (2012) 893–916, https://doi.org/10.1111/j.1574-6976.2011.00322.x.
[47] H.C. Flemming, J. Wingender, The biofilm matrix, Nat. Rev. Microbiol. 8 (9) (2010) 623–633, https://doi.org/10.1038/nrmicro2415.
[48] I.L.S. Chua, H.W. Kim, J.H. Lee, Signaling of extracellular matrices for tissue regeneration and therapeutics, Tissue Eng. Regen. Med. 13 (1) (2016) 1–12, https://doi.org/10.1007/s13770-016-9075-0.
[49] W. Han, N.K. Singh, J.J. Kim, H. Kim, B.S. Kim, J.Y. Park, J. Jang, D.W. Cho, Directed differential behaviors of multipotent adult stem cells from decellularized tissue/organ extracellular matrix bioinks, Biomaterials 224 (2019) 119496, , https://doi.org/10.1016/j.biomaterials.2019.119496 UNSP 119496.
[50] F. Pati, J. Jang, D.H. Ha, S. Won Kim, J.W. Rhie, J.H. Shim, D.H. Kim, D.W. Cho, Printing three-dimensional tissue analogues with decellularized extracellular matrix bioink, Nat. Commun. 5 (2014) 3935, https://doi.org/10.1038/ncomms4935.
[51] J.M. Aamodt, D.W. Grainger, Extracellular matrix-based biomaterial scaffolds and the host response, Biomaterials 86 (2016) 68–82, https://doi.org/10.1016/j.biomaterials.2016.02.003.
[52] R. Raghunathan, M.K. Sethi, J.A. Klein, J. Zaia, Proteomics, glycomics, and glycoproteomics of matrisome molecules, Mol. Cell. Proteomics 18 (11) (2019) 2138–2148, https://doi.org/10.1074/mcp.R119.001543.
[53] H. Bi, K. Ye, S. Jin, Proteomic analysis of decellularized pancreatic matrix identifies collagen V as a critical regulator for islet organogenesis from human pluripotent stem cells, Biomaterials 233 (2020) 119673, , https://doi.org/10.1016/j.biomaterials.2019.119673.
[54] H. Ragelle, A. Naba, B.L. Larson, F. Zhou, M. Prijic, C.A. Whittaker, A. Del Rosario, R. Langer, R.O. Hynes, D.G. Anderson, Comprehensive proteomic characterization of stem cell-derived extracellular matrices, Biomaterials 128 (2017) 147–159, https://doi.org/10.1016/j.biomaterials.2017.03.008.
[55] Q.Y. Li, B.E. Uygun, S. Geerts, S. Ozer, M. Scalf, S.E. Gilpin, H.C. Ott, M.L. Yarmush, L.M. Smith, N.V. Welham, B.L. Frey, Proteomic analysis of naturally-sourced biological scaffolds, Biomaterials 75 (2016) 37–46, https://doi.org/10.1016/j.biomaterials.2015.10.011.
[56] M. Baroncelli, B.C. van der Eerden, Y.Y. Kan, R.D. Alves, J.A. Demmers, J. van de Peppel, J.P. van Leeuwen, Comparative proteomic profiling of human osteoblast-derived extracellular matrices identifies proteins involved in mesenchymal stromal cell osteogenic differentiation and mineralization, J. Cell. Physiol. 233 (1) (2018) 387–395, https://doi.org/10.1002/jcp.25898.
[57] P. Zhu, Y.Y. Goh, H.F. Chin, S. Kersten, N.S. Tan, Angiopoietin-like 4: a decade of research, Biosci. Rep. 32 (3) (2012) 211–219, https://doi.org/10.1042/BSR20110102.
[58] K. Janjic, A. Schellner, A. Engenhart, K. Kernstock, B. Schadl, A. Moritz, H. Agis, Angiopoietin-like 4 production upon treatment with hypoxia and L-mimosine in periodontal fibroblasts, J. Periodontal. Res. 54 (5) (2019) 489–498, https://doi.org/10.1111/jre.12649.
[59] U. Schwarze, T. Cundy, Y.J. Liu, P.L. Hofman, P.H. Byers, Compound heterozygosity for a frameshift mutation and an upstream deletion that reduces expression of SERPINH1 in siblings with a moderate form of osteogenesis imperfecta, Am. J. Med. Genet. 179 (8) (2019) 1466–1475, https://doi.org/10.1002/ajmg.a.61170.